New Journal of Physics

The open access journal at the forefront of physics

PAPER

Light interaction with extended quantum systems in dispersive media

Giovanni Scala[1,2] , Francesco V Pepe[1,2,*] , Paolo Facchi[1,2] , Saverio Pascazio[1,2] and Karolina Słowik[3]

1 Dipartimento di Fisica and MECENAS, Università di Bari, I-70126 Bari, Italy
2 INFN, Sezione di Bari, I-70125 Bari, Italy
3 Institute of Physics, Nicolaus Copernicus University in Toruń, Grudziadzka 5, 87-100 Torun, Poland
* Author to whom any correspondence should be addressed.

E-mail: francesco.pepe@ba.infn.it

Abstract

We derive a light–matter interaction Hamiltonian to describe a quantum system embedded in a dispersive environment and coupled with the electromagnetic field. We include in this theory the spatial extension of the system, taken into account through its wavefunction. This enables us to overcome the diver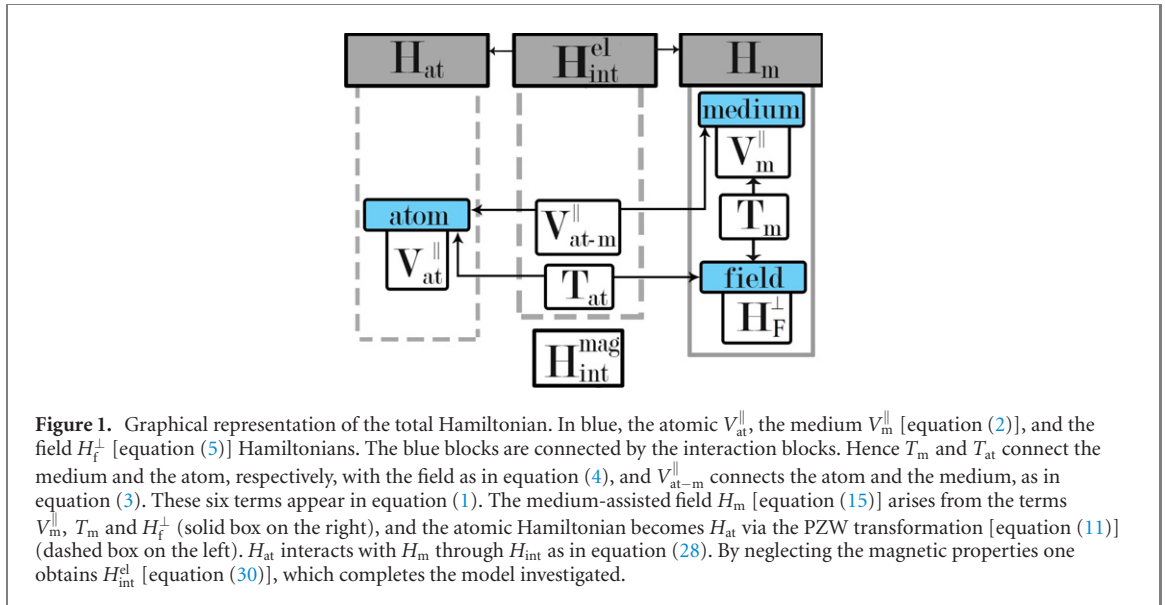gence problem of the Green tensor propagator that arises from a point-like approximation of the quantum system. Thus the formalism can be applied to generalize the expressions for the spontaneous emission rate and the Lamb shift for a quantum system defined by a spatially extended dipole. In particular, these quantities can be modified by the asymmetry of the spatial structure of the atomic system as demonstrated in two test-bed examples.

1. Introduction

The interaction of an atomic system with a surrounding photonic bath yields a correction to the atomic transition energy, referred to as Lamb shift [1], and gives rise to the process of spontaneous emission. The latter is described in the Markovian limit as an exponential decay [2, 3], while a much more sophisticated behavior was predicted and verified in non-Markovian regimes [4, 5]. If multiple emitters are present, a shared photonic bath acts as a carrier of interactions among them and is responsible for collective emission, such as Casimir effect [6] or Dicke superradiance [7]. For a comprehensive discussion of these and other effects of quantum vacuum on atomic systems see [8].

The spatial and spectral structure of the photonic bath can be tailored, e.g. with traditional cavities or nanostructured materials. As a consequence, the effects arising in atomic systems coupled to such tailored surroundings are modified accordingly [9, 10]. When it comes to spontaneous emission, this phenomenon has been termed Purcell effect [11–14]. Similarly, the Lamb shift and collective effects can be tailored by proper engineering of the photonic bath [15, 16]. In the great majority of works studying light–matter interactions in this context, atomic systems are assumed to be point-like dipoles, without internal structure. This is usually a well-justified approximation, since the size of the atomic system is much below the emission wavelength. However, recent advancement in the field of nanophotonic brought into reach nano- or even picometric cavities [17, 18]. In the conditions of extreme light confinement, the internal structure of the atomic system might have a considerable impact on its optical response, which might require extensions of the theory beyond the point-dipole [19–21] or electric-dipole approximations [22]. On the other hand, spatially extended systems like quantum dots may require such treatment even when embedded in a photonic environment as simple as a homogeneous and isotropic medium.

Accounting for the internal structure of atomic systems can lead to much more than quantitative corrections of their optical properties; actually, effects like spatial asymmetry may give rise to appealing new applications, such as optically-tunable low-frequency radiation sources based on resonantly driven systems [23–25]. Scenarios exploiting systems with broken inversion symmetry were proposed for light squeezing

Figure 1. Graphical representation of the total Hamiltonian. In blue, the atomic $V_{at}^{\parallel}$, the medium $V_{m}^{\parallel}$ [equation (2)], and the field $H_{f}^{\perp}$ [equation (5)] Hamiltonians. The blue blocks are connected by the interaction blocks. Hence T_{m} and T_{at} connect the medium and the atom, respectively, with the field as in equation (4), and $V_{at-m}^{\parallel}$ connects the atom and the medium, as in equation (3). These six terms appear in equation (1). The medium-assisted field H_{m} [equation (15)] arises from the terms $V_{m}^{\parallel}$, T_{m} and $H_{f}^{\perp}$ (solid box on the right), and the atomic Hamiltonian becomes H_{at} via the PZW transformation [equation (11)] (dashed box on the left). H_{at} interacts with H_{m} through H_{int} as in equation (28). By neglecting the magnetic properties one obtains H_{int}^{el} [equation (30)], which completes the model investigated.

[26] and lasing [27]. The asymmetry has already been studied in the context of a coherent driving field [28, 29] with a long list of recent experiments which involve quantum piezoelectricity [30], quantum dots [30], dye molecules [31], spin-echo [32], Ramsey interferometer [33], crystal centers [13, 34], and graphene [35, 36].

We shall avoid the introduction of ad hoc artificial cutoffs to remove the divergencies that arise, in the context analyzed in this article, from two distinct effects: the assumption of point-like atoms and the neglection of the medium granularity, which amounts to disregarding the momentum-dependence of the dielectric permittivity. Observe that the different nature of these divergences is lost if an artificial cutoff is introduced. We propose here an approach in which the wavefunctions are consistently incorporated in the description of the system and in the determination of the decay rates and Lamb shifts. This enables us to describe in a natural way all effects due to anisotropies and the broken inversion symmetry. Our results will therefore be valid (and of special interest) in the context of artificial atoms, in which the wavefunctions can in principle extend beyond medium granularity, therefore providing the essential natural cutoff to the system. As opposed to artificial cutoffs, this method provides reliable results also for near field.

We shall see how the divergence problem [37, 38], encountered when one evaluates the transition properties of atomic systems in dispersive media, can be solved naturally. This problem was treated with many different approaches in other works [39–42]. We shall exploit the medium-assisted field expressed through the Green tensor propagator [43, 44], which can be applied also for classical electrodynamics [45], to account for the properties of the photonic surroundings. These can be modified in presence of a host medium, which in general could be structured in terms of geometric shape and spectral response. Although parts of our theory are general, we pay special attention to translationally invariant media.

The article is organized as follows. In section 2, we discuss all the terms of the Hamiltonian; in particular, we describe the form of the coupling between a system of charges and a medium-assisted field, representing in a single entity both the electromagnetic field and the medium charges. In section 3, we use the developed theory to obtain the decay rate and energy shift for an arbitrary bound state, highlighting the contribution of spatial asymmetry of the eigenstates of the atomic Hamiltonian. In section 4, we apply the results to two test-beds. Finally, in section 5, we summarize the obtained results and outline future research.

2. Hamiltonian

We start from a first-principle Hamiltonian where positive and negative charges of the atomic system and the medium are coupled with the electromagnetic field. If the focus is on the atomic dynamics, the system can be conveniently modeled by coupling the atom to a *medium-assisted* electromagnetic field, which is dressed by the interaction with the hosting medium (see figure 1).

Let us consider the Coulomb-gauge Hamiltonian [46, 47], separating the longitudinal and transverse contributions

$$H = V_{at}^{\parallel} + V_{m}^{\parallel} + V_{at-m}^{\parallel} + T_{at} + T_{m} + H_{F}^{\perp}. \tag{1}$$

Atomic charges will be labelled by roman indices j, k and the charges of the medium by Greek indices μ, ν. The terms

$$V_{\mathrm{at}}^{\|} = \frac{1}{8\pi\epsilon_0} \sum_{j \neq k} \frac{Q_j Q_k}{|\boldsymbol{r}_j - \boldsymbol{r}_k|}, \qquad V_{\mathrm{m}}^{\|} = \frac{1}{8\pi\epsilon_0} \sum_{\mu \neq \nu} \frac{Q_\mu Q_\nu}{|\boldsymbol{r}_\mu - \boldsymbol{r}_\nu|}, \tag{2}$$

represent the internal Coulomb interactions among the charges Q_k of the atomic system (placed at positions $\boldsymbol{r}_k$) and among the charges Q_μ of the medium (placed at positions $\boldsymbol{r}_\mu$), respectively. The atom–medium Coulomb interactions read

$$V_{\mathrm{at-m}}^{\|} = \frac{1}{4\pi\epsilon_0} \sum_{j,\mu} \frac{Q_j Q_\mu}{|\boldsymbol{r}_j - \boldsymbol{r}_\mu|}. \tag{3}$$

The kinetic terms

$$T_{\mathrm{at}} = \sum_j \frac{\left(\boldsymbol{p}_j - Q_j \boldsymbol{A}(\boldsymbol{r}_j)\right)^2}{2m_j}, \qquad T_{\mathrm{m}} = \sum_\mu \frac{\left(\boldsymbol{p}_\mu - Q_\mu \boldsymbol{A}(\boldsymbol{r}_\mu)\right)^2}{2m_\mu}, \tag{4}$$

contain the minimal coupling between the charges (with canonical momenta $\boldsymbol{p}_j = -i\hbar\nabla_{\boldsymbol{r}_j}$ and $\boldsymbol{p}_\mu = -i\hbar\nabla_{\boldsymbol{r}_\mu}$, and masses m_j and m_μ, respectively) and the transverse part of the field, represented by the Coulomb gauge vector potential $\boldsymbol{A}$ (purely transverse, $\nabla \cdot \boldsymbol{A} = 0$). Finally,

$$H_{\mathrm{F}}^{\perp} = \frac{1}{2} \int \mathrm{d}^3\boldsymbol{r} \left(\epsilon_0 \dot{\boldsymbol{A}}^2(\boldsymbol{r}) + \frac{1}{\mu_0} [\nabla \times \boldsymbol{A}(\boldsymbol{r})]^2 \right) \tag{5}$$

is the Hamiltonian of the free field in vacuum. If one considers a neutral atom, the charge density

$$\rho_{\mathrm{at}}(\boldsymbol{r}) = \sum_j Q_j \delta(\boldsymbol{r} - \boldsymbol{r}_j), \quad \text{with} \sum_j Q_j = 0, \tag{6}$$

can be expressed as the divergence of a polarization density $\rho_{\mathrm{at}}(\boldsymbol{r}) = -\nabla \cdot \boldsymbol{P}_{\mathrm{at}}(\boldsymbol{r})$. Here,

$$\boldsymbol{P}_{\mathrm{at}}(\boldsymbol{r}) = \sum_j q_j \int_0^1 \mathrm{d}s\, (\boldsymbol{r}_j - \boldsymbol{R}) \delta(\boldsymbol{r} - \boldsymbol{R} - s(\boldsymbol{r}_j - \boldsymbol{R})), \tag{7}$$

where $\boldsymbol{R}$ is the center-of-mass coordinate [47]. The atomic polarization density allows us to express the Coulomb interaction terms as follows

$$V_{\mathrm{at}}^{\|} = \frac{1}{2\epsilon_0} \int \mathrm{d}^3\boldsymbol{r} \left(\boldsymbol{P}_{\mathrm{at}}^{\|}(\boldsymbol{r}) \right)^2, \tag{8}$$

$$V_{\mathrm{at-m}}^{\|} = \frac{1}{\epsilon_0} \int \mathrm{d}^3\boldsymbol{r}\, \boldsymbol{P}_{\mathrm{at}}^{\|}(\boldsymbol{r}) \cdot \boldsymbol{\Pi}^{\|}(\boldsymbol{r}). \tag{9}$$

Here, $\boldsymbol{P}_{\mathrm{at}}^{\|}$ is the longitudinal part of the polarization, i.e. the only component that determines the atomic charge density, and $\boldsymbol{\Pi}^{\|}$ is the longitudinal displacement field of the medium, that satisfies

$$\nabla \cdot \boldsymbol{\Pi}^{\|}(\boldsymbol{r}) = -\sum_\mu Q_\mu \delta(\boldsymbol{r} - \boldsymbol{r}_\mu). \tag{10}$$

The latter is proportional to the Coulomb field $\boldsymbol{E}^{\|} = -\boldsymbol{\Pi}^{\|}/\epsilon_0$ generated by the medium charges.

2.1. Minimal coupling

We now analyze the coupling between the atom and the electromagnetic field, which is a consequence of the minimal coupling in the kinetic energy terms in equation (4). For an atom modeled as a point-like dipole, it is possible to shift from the '$\boldsymbol{p} \cdot \boldsymbol{A}$' to the '$\boldsymbol{r} \cdot \boldsymbol{E}$' coupling representation, through the unitary transformation $\exp(-iQ\boldsymbol{r} \cdot \boldsymbol{A}/\hbar)$, where the vector potential is computed at the dipole center of mass [47]. The advantage of this transformation lies in the fact that, in the transformed picture, the canonical momentum of a particle coincides with its kinetic momentum and it is decoupled from the field variables (a thorough discussion of the implications of such a feature is given in reference [47]).

In the case of a finite-size dipole, the aforementioned unitary transformation generalizes to the Power–Zienau–Wolley (PZW) operator [46, 47]:

$$U_{\mathrm{PZW}} = \exp\left(-\frac{i}{\hbar} \int \mathrm{d}^3\boldsymbol{r}\, \boldsymbol{P}_{\mathrm{at}}(\boldsymbol{r}) \cdot \boldsymbol{A}(\boldsymbol{r}) \right) = \exp\left(-\frac{i}{\hbar} \int \mathrm{d}^3\boldsymbol{r}\, \boldsymbol{P}_{\mathrm{at}}^{\perp}(\boldsymbol{r}) \cdot \boldsymbol{A}^{\perp}(\boldsymbol{r}) \right). \tag{11}$$

The transformation property $U_{\mathrm{PZW}}\mathbf{\Pi}^{\perp}(\mathbf{r})U_{\mathrm{PZW}}^{\dagger} = \mathbf{\Pi}^{\perp}(\mathbf{r}) + \mathbf{P}_{\mathrm{at}}^{\perp}(\mathbf{r})$ yields two transverse-field terms from equation (5)

$$V_{\mathrm{at}}^{\perp} = \frac{1}{2\epsilon_0}\int \mathrm{d}^3\mathbf{r}\left(\mathbf{P}_{\mathrm{at}}^{\perp}(\mathbf{r})\right)^2, \qquad V_{\mathrm{at-m}}^{\perp} = \frac{1}{\epsilon_0}\int \mathrm{d}^3\mathbf{r}\,\mathbf{P}_{\mathrm{at}}^{\perp}(\mathbf{r})\cdot \mathbf{\Pi}^{\perp}(\mathbf{r}). \tag{12}$$

These contributions are complementary to the ones in equations (8) and (9). The latter, as well as the transverse part of the atomic polarization density, are instead left unchanged by the transformation. Although originally $\mathbf{\Pi}^{\perp} = -\epsilon_0 \mathbf{E}^{\perp}$, the proportionality is lost after the transformation

$$\mathbf{\Pi}(\mathbf{r}) = -\epsilon_0 U_{\mathrm{PZW}}\mathbf{E}(\mathbf{r})U_{\mathrm{PZW}}^{\dagger} - U_{\mathrm{PZW}}\mathbf{P}_{\mathrm{at}}(\mathbf{r})U_{\mathrm{PZW}}^{\dagger}, \tag{13}$$

which can be shown using equation (10). For a finite-size dipole, the equality between the kinetic and canonical momenta is not exactly realized in the transformed frame as in the case of a point-like dipole transformation. The reason is that the transformed kinetic momentum

$$U_{\mathrm{PZW}}(\mathbf{p}_j + Q_j\mathbf{A}(\mathbf{r}_j))U_{\mathrm{PZW}}^{\dagger} = \mathbf{p}_j + Q_j\int_0^1 \mathrm{d}s\, s(\mathbf{r}_j - \mathbf{R})\mathbf{B}(\mathbf{R} + s(\mathbf{r}_j - \mathbf{R})) \tag{14}$$

acquires an additional term, which generates a direct coupling between the charges and the magnetic field $\mathbf{B}$. Nevertheless, the difference between the two momenta in the transformed representation is suppressed with respect to the analogous difference in the Coulomb gauge as the ratio between the atomic size and the interacting light wavelength. Therefore, if one neglects the interaction with the magnetic field, it can be consistently assumed that $\mathbf{p}_j$ coincides with the jth particle kinetic momentum in the transformed representation.

2.2. Medium-assisted electromagnetic field

The medium-assisted electromagnetic field is an effective model that conveniently describes, under certain approximations, the combination of the medium and the field degrees of freedom, as pictured in figure 1. The contributions to the medium-assisted Hamiltonian arise from the terms $V_{\mathrm{m}}^{\parallel}$, T_{m} and $H_{\mathrm{F}}^{\perp}$ in the Hamiltonian (1), as derived in detail in references [41, 48, 49]. The resulting effective field Hamiltonian,

$$H_{\mathrm{m}} = \int_0^{\infty} \mathrm{d}\omega \int \mathrm{d}^3\mathbf{r}\,\hbar\omega \mathbf{f}^{\dagger}(\mathbf{r},\omega)\cdot \mathbf{f}(\mathbf{r},\omega), \tag{15}$$

can be expanded in three-component mode operators $\mathbf{f}(\mathbf{r},\omega)$ and $\mathbf{f}^{\dagger}(\mathbf{r},\omega)$, satisfying canonical commutation relations

$$\left[f_k\left(\mathbf{r},\omega\right),f_{k'}^{\dagger}\left(\mathbf{r}',\omega'\right)\right] = \delta_{kk'}\delta\left(\mathbf{r}-\mathbf{r}'\right)\delta\left(\omega-\omega'\right),$$

$$\left[f_k\left(\mathbf{r},\omega\right),f_{k'}\left(\mathbf{r}',\omega'\right)\right] = \left[f_k^{\dagger}\left(\mathbf{r},\omega\right),f_{k'}^{\dagger}\left(\mathbf{r}',\omega'\right)\right] = 0, \tag{16}$$

with $k = 1,2,3$.

The displacement field $\mathbf{\Pi}$ and the vector potential $\mathbf{A}$ are related to the field variable $\mathbf{f}$ by

$$\Pi_j(\mathbf{r}) = \int_0^{\infty} \mathrm{d}\omega \int \mathrm{d}^3\mathbf{r}'\left[-\mathrm{i}\frac{\omega^2}{c^2}\sqrt{\frac{\hbar\epsilon_0}{\pi}\epsilon_{\mathrm{I}}(\mathbf{r}',\omega)}G_{jk}(\mathbf{r},\mathbf{r}',\omega)f_k(\mathbf{r}',\omega) + \mathrm{H.c.}\right], \tag{17}$$

$$A_j(\mathbf{r}) = \int_0^{\infty} \mathrm{d}\omega \int \mathrm{d}^3\mathbf{r}'\left[\frac{\omega}{c^2}\sqrt{\frac{\hbar}{\pi\epsilon_0}\epsilon_{\mathrm{I}}(\mathbf{r}',\omega)}G_{jk}^{\perp}(\mathbf{r},\mathbf{r}',\omega)f_k(\mathbf{r}',\omega) + \mathrm{H.c.}\right], \tag{18}$$

where ϵ_{I} is the imaginary part of the dielectric permittivity

$$\epsilon(\mathbf{r},\omega) = \epsilon_{\mathrm{R}}(\mathbf{r},\omega) + \mathrm{i}\epsilon_{\mathrm{I}}(\mathbf{r},\omega). \tag{19}$$

We have assumed that the medium is isotropic, hence the permittivity is a scalar. The Green tensor G appearing in equation (17) is the solution of the equation [46]

$$\left[\partial_j\partial_\ell - \delta_{j\ell}\left(\nabla^2 + \frac{\omega^2}{c^2}\epsilon(\mathbf{r},\omega)\right)\right]G_{\ell k}(\mathbf{r},\mathbf{r}',\omega) = \delta_{jk}\delta(\mathbf{r}-\mathbf{r}'), \tag{20}$$

and the term $G^{\perp}$ in equation (18) represents its transverse part, satisfying $\partial G_{\ell k}^{\perp}(\mathbf{r},\mathbf{r}',\omega)/\partial r_{\ell} = \partial G_{k\ell}^{\perp}(\mathbf{r}',\mathbf{r},\omega)/\partial r_{\ell}' = 0$. In the Coulomb gauge, the properties of the Green tensor and the analytic structure of

$\epsilon(\boldsymbol{r}, \omega)$ in the complex frequency plane guarantee that the vector potential and the transverse part of the displacement field satisfy the canonical commutation relations

$$\left[A_j(\boldsymbol{r}), \Pi_k(\boldsymbol{r}')\right] = \mathrm{i}\hbar\delta_{jk}^{\perp}(\boldsymbol{r} - \boldsymbol{r}') = \mathrm{i}\hbar \int \frac{\mathrm{d}^3\boldsymbol{q}}{(2\pi)^3} \left(\delta_{j\ell} - \frac{q_j q_\ell}{|\boldsymbol{q}|^2}\right) \mathrm{e}^{\mathrm{i}\boldsymbol{q}\cdot(\boldsymbol{r}-\boldsymbol{r}')}. \tag{21}$$

For a translationally invariant medium, $\epsilon(\boldsymbol{r}, \omega) = \epsilon(\omega)$, thus the Green tensor depends only on the coordinate difference, $G(\boldsymbol{r}, \boldsymbol{r}', \omega) = G(\boldsymbol{r} - \boldsymbol{r}', \omega)$, and its Fourier transform

$$\tilde{G}_{jk}(\boldsymbol{q}, \omega) = \int \mathrm{d}^3\boldsymbol{r}\, G_{jk}(\boldsymbol{r}, \omega)\mathrm{e}^{-\mathrm{i}\boldsymbol{q}\cdot\boldsymbol{r}}, \tag{22}$$

reads

$$\tilde{G}_{jk}^{\perp}(\boldsymbol{q}, \omega) = \left(\delta_{j\ell} - \frac{q_j q_\ell}{|\boldsymbol{q}|^2}\right) \tilde{G}_{\ell k}(\boldsymbol{q}, \omega) = \frac{\delta_{jk} - q_j q_k/|\boldsymbol{q}|^2}{|\boldsymbol{q}|^2 - \omega^2\epsilon(\omega)/c^2},$$

$$\tilde{G}_{jk}^{\parallel}(\boldsymbol{q}, \omega) = \frac{q_j q_\ell}{|\boldsymbol{q}|^2} \tilde{G}_{\ell k}(\boldsymbol{q}, \omega) = -\frac{q_j q_k}{|\boldsymbol{q}|^2} \frac{c^2}{\omega^2\epsilon(\omega)}. \tag{23}$$

Hence, the displacement field reduces to

$$\Pi_j(\boldsymbol{r}) = \int_0^\infty \mathrm{d}\omega \int \frac{\mathrm{d}^3\boldsymbol{q}}{(2\pi)^3} \left[-\mathrm{i}\frac{\omega^2}{c^2}\sqrt{\frac{\hbar\epsilon_0}{\pi}}\epsilon_{\mathrm{I}}(\omega)\tilde{G}_{jk}(\boldsymbol{q}, \omega)\tilde{f}_k(\boldsymbol{q}, \omega)\mathrm{e}^{\mathrm{i}\boldsymbol{q}\cdot\boldsymbol{r}} + \mathrm{H.c.}\right], \tag{24}$$

where the operators

$$\tilde{\boldsymbol{f}}(\boldsymbol{q}, \omega) = \int \mathrm{d}^3\boldsymbol{r}\, \boldsymbol{f}(\boldsymbol{r}, \omega)\mathrm{e}^{-\mathrm{i}\boldsymbol{q}\cdot\boldsymbol{r}}, \tag{25}$$

satisfy

$$[\tilde{f}_j(\boldsymbol{q}, \omega), \tilde{f}_k^\dagger(\boldsymbol{q}', \omega')] = (2\pi)^3 \delta_{jk}\delta(\omega - \omega')\delta(\boldsymbol{q} - \boldsymbol{q}'). \tag{26}$$

For a point-like atomic system, singularities may arise in the interaction Hamiltonian due to the fact that the quantities $G^{\parallel}(\boldsymbol{r}, \omega)$ and $G^{\perp}(\boldsymbol{r}, \omega)$ diverge as $\boldsymbol{r} \to \boldsymbol{0}$. In fact, while

$$\mathrm{Im}G_{jk}^{\perp}(\boldsymbol{0}, \omega) = \int \frac{\mathrm{d}^3\boldsymbol{q}}{(2\pi)^3} \mathrm{Im}\tilde{G}_{jk}^{\perp}(\boldsymbol{q}, \omega) = \frac{\omega^2\epsilon_{\mathrm{I}}(\omega)}{c^2} \int \frac{\mathrm{d}^3\boldsymbol{q}}{(2\pi)^3} \frac{\delta_{jk} - q_j q_k/|\boldsymbol{q}|^2}{\left||\boldsymbol{q}|^2 - \frac{\omega^2\epsilon(\omega)}{c^2}\right|^2} \tag{27}$$

is finite and yields a well-defined transverse decay rate [41], $\mathrm{Im}\, G^{\parallel}(\boldsymbol{r}, \omega)$ diverges as $\boldsymbol{r} \to \boldsymbol{0}$, due to the non integrability of $\mathrm{Im}\, \tilde{G}_{jk}^{\parallel}(\boldsymbol{q}, \omega) \propto q_j q_k/|\boldsymbol{q}|^2$, and a consistent treatment of the longitudinal decay rate requires momentum regularization.

Techniques based on considering the source enclosed in an artificial cavity [40, 50, 51] have been developed to cope with such singularities. In the following, we will tackle the divergences of the longitudinal part with a less artificial approach, by considering the natural finite spatial extent of the atomic wavefunctions. This will allow us to unambiguously analyze the role of the asymmetry of the atomic states on the emission process.

2.3. Total Hamiltonian
From the previous parts of this section it follows that

$$H = H_{\mathrm{at}} + H_{\mathrm{int}}^{\mathrm{el}} + H_{\mathrm{int}}^{\mathrm{mag}} + H_{\mathrm{m}}. \tag{28}$$

Here,

$$H_{\mathrm{at}} = H_{\mathrm{at}}^0 + V_{\mathrm{at}} = \sum_j \frac{\boldsymbol{p}_j^2}{2m_j} + \frac{1}{2\epsilon_0} \int \mathrm{d}^3\boldsymbol{r}\, (\boldsymbol{P}_{\mathrm{at}}(\boldsymbol{r}))^2 \tag{29}$$

is the atomic Hamiltonian,

$$H_{\mathrm{int}}^{\mathrm{el}} = \frac{1}{\epsilon_0} \int \mathrm{d}^3\boldsymbol{r}\, \boldsymbol{P}_{\mathrm{at}}(\boldsymbol{r}) \cdot \boldsymbol{\Pi}(\boldsymbol{r}) = \frac{1}{\epsilon_0} \sum_j Q_j(\boldsymbol{r}_j - \boldsymbol{R}) \cdot \int \mathrm{d}s\, \boldsymbol{\Pi}(\boldsymbol{R} + s(\boldsymbol{r}_j - \boldsymbol{R})) \tag{30}$$

represents the interaction of the atomic system with the electric field, and

$$H_{\text{int}}^{\text{mag}} = \sum_j \left\{ \frac{Q_j}{m_j} \boldsymbol{p}_j \cdot \int_0^1 \mathrm{d}s\, s(\boldsymbol{r}_j - \boldsymbol{R}) \boldsymbol{B}(\boldsymbol{R} + s(\boldsymbol{r}_j - \boldsymbol{R})) \right.$$

$$\left. + \frac{Q_j^2}{2m_j} \left[\int_0^1 \mathrm{d}s\, s(\boldsymbol{r}_j - \boldsymbol{R}) \boldsymbol{B}(\boldsymbol{R} + s(\boldsymbol{r}_j - \boldsymbol{R})) \right]^2 \right\} \tag{31}$$

stands for the coupling with the magnetic field. The term H_{m} generally represents the Hamiltonian of the medium, that can be modeled in different ways, e.g. through the medium-assisted field Hamiltonian (15), as shown in section 2.2. In the following part of this work we will neglect the magnetic contribution to the interaction. Now we model the atom of the general theory as an electric dipole of charge Q, with a heavy positive charge at the fixed position $\boldsymbol{R} = 0$ and a moving negative charge of coordinate $-\boldsymbol{r}$ and mass m. As a result, one finds the final form of the interaction Hamiltonian

$$H_{\text{int}}^{\text{dip}} = \frac{Q}{\epsilon_0} \boldsymbol{r} \cdot \int_0^1 \mathrm{d}s\, \boldsymbol{\Pi}(-s\boldsymbol{r}), \tag{32}$$

representing the correct generalization of the '$\boldsymbol{r} \cdot \boldsymbol{E}$' Hamiltonian to an extended (non point-like) dipole.

The expression (17) of the displacement field $\boldsymbol{\Pi}$ in terms of the Green tensor in the Hamiltonian $H_{\text{int}}^{\text{dip}}$ provides a new accurate and general approach. In the following examples we apply the general theory in the simple case of a homogeneous medium. However, by exploiting the tensor structure one can consider various geometries of the host medium, in particular interfaces of different dimensions or photonic nanostructures. The use of the Green's tensor leads to a divergent field at the position of the point-like quantum system. This divergence is usually removed in a somewhat artificial way by introducing virtual cavities or form factors. Here, the renormalization procedure is based on the physical size and orientation of the extended system represented with wavefunctions. It allows us to accurately describe the physics of the system without artefacts. This is one of the main findings of this work, that arises as a connection between first-principle QED, represented through the canonical commutation relations, and the medium-assisted field ruled by equation (16).

3. Emission properties of a bound system of charges

According to the results of the previous section, each eigenstate of the internal atomic Hamiltonian is dressed by the surrounding medium. We now characterize the single-photon emission process and the Lamb shift of an atomic level in a medium-assisted photonic environment in a translationally invariant medium.

Consider an atom in an arbitrary environment, i.e. a dispersive medium of any geometry and material. Let $|a\rangle$ and $|b\rangle$ be two orthogonal eigenstates of the free atomic Hamiltonian H_{at}, characterized by

$$H_{\text{at}}|a\rangle = E_a|a\rangle, \qquad H_{\text{at}}|b\rangle = E_b|b\rangle. \tag{33}$$

The atom–photon interaction is described by the matrix element

$$\mathcal{M}_j^{ab}(\boldsymbol{r}, \omega) = \langle a | H_{\text{int}}^{\text{dip}} f_j^\dagger(\boldsymbol{r}, \omega) | b \rangle, \tag{34}$$

which, for a translationally-invariant medium, can be expressed in the Fourier space through

$$\tilde{\mathcal{M}}_j^{ab}(\boldsymbol{q}, \omega) = \langle a | H_{\text{int}}^{\text{dip}} \tilde{f}_j^\dagger(\boldsymbol{q}, \omega) | b \rangle = -\mathrm{i}C(\omega) \frac{\omega^2}{c^2} \sum_k \tilde{G}_{jk}(\boldsymbol{q}, \omega) \langle a | r_k \int_0^1 \mathrm{d}s\, \mathrm{e}^{-\mathrm{i}s\boldsymbol{q}\cdot\boldsymbol{r}} | b \rangle, \tag{35}$$

where

$$C(\omega) = Q\sqrt{\frac{\hbar\epsilon_{\text{I}}(\omega)}{8\pi^4\epsilon_0}}.$$

If we insert the expression of $\tilde{G}_{jk}$ in equation (23) and exploit the orthogonality between longitudinal and transverse projectors, we obtain

$$\mathcal{T}_{ab}(\boldsymbol{q}, \omega) = \sum_{j=1}^3 \left| \tilde{\mathcal{M}}_j^{ab}(\boldsymbol{q}, \omega) \right|^2$$

$$= \frac{C(\omega)^2}{|\epsilon(\omega)|^2} \left[\mathcal{D}(|\boldsymbol{q}|, \omega) \mathcal{G}_{ab}(\boldsymbol{q}) + (1 - \mathcal{D}(|\boldsymbol{q}|, \omega)) \frac{|\mathcal{F}_{ab}(\boldsymbol{q}) - \delta_{ab}|^2}{|\boldsymbol{q}|^2} \right], \tag{36}$$

where $\delta_{ab} = \langle a|b \rangle = 1$ if $|a\rangle$ and $|b\rangle$ coincide and 0 otherwise, with

$$\mathcal{D}(q,\omega) = \left| 1 - \frac{q^2 c^2}{\omega^2 \epsilon(\omega)} \right|^{-2}, \tag{37}$$

$$\mathcal{F}_{ab}(\boldsymbol{q}) = \langle a|e^{-i\boldsymbol{q}\cdot\boldsymbol{r}}|b\rangle = \int d^3\boldsymbol{r}\, \psi_a^*(\boldsymbol{r})\psi_b(\boldsymbol{r})e^{-i\boldsymbol{q}\cdot\boldsymbol{r}}, \tag{38}$$

$$\mathcal{G}_{ab}(\boldsymbol{q}) = \sum_{j=1}^{3} \left| \langle a|r_j \frac{e^{-i\boldsymbol{q}\cdot\boldsymbol{r}} - 1}{\boldsymbol{q}\cdot\boldsymbol{r}}|b\rangle \right|^2. \tag{39}$$

The quantity defined in equation (36) determines both the total decay rate of the state $|a\rangle$ and its energy shift. The former can be evaluated according to the Fermi golden rule

$$
\begin{aligned}
\Gamma_a &= \frac{2\pi}{\hbar} \sum_b \int_0^\infty d\omega\, \delta(\hbar\omega - \hbar\omega_{ab}) T_{ab}(\omega) = \frac{2\pi}{\hbar^2} \sum_{b\neq a} \theta(\omega_{ab}) T_{ab}(\omega_{ab}) \\
&= \frac{2\pi}{\hbar^2} \sum_{b\neq a} \theta(\omega_{ab}) \frac{C(\omega_{ab})^2}{|\epsilon(\omega_{ab})|^2} \int d^3\boldsymbol{q} \left[\mathcal{D}(|\boldsymbol{q}|,\omega_{ab})\mathcal{G}_{ab}(\boldsymbol{q}) + (1 - \mathcal{D}(|\boldsymbol{q}|,\omega_{ab}))\frac{|\mathcal{F}_{ab}(\boldsymbol{q})|^2}{|\boldsymbol{q}|^2} \right],
\end{aligned}
\tag{40}
$$

with

$$\omega_{ab} = \frac{E_a - E_b}{\hbar}, \qquad T_{ab}(\omega) = \int d^3\boldsymbol{q}\, \mathcal{T}_{ab}(\boldsymbol{q},\omega), \tag{41}$$

and $\theta(x)$ being the Heaviside step function. The absence of a contribution from state $|a\rangle$ in the sum over states in the second equality of equation (40), albeit reasonable, is not a trivial result. Therefore, replacing equation (36) in the evaluation of the decay rate $\delta_{ab} = 0$ and the apparent divergence in the term proportional to $\mathcal{F}_{ab}$ is regularized by the wavefunctions spatial extension. Note that the two terms in equation (40) proportional to $\mathcal{D}(q,\omega)$ correspond to the transverse contribution, while the remaining one is the longitudinal contribution responsible for non-radiative decay, because it is related to the absorption losses in the dielectric host medium.

In vacuum ($\epsilon(\omega) = 1$), the decay rate in equation (40) becomes

$$\Gamma_a^{(\text{vac})} = \frac{Q^2 q^3}{8\pi^2 \hbar\epsilon_0} \int_{\mathbb{S}^2} d^2 S(\boldsymbol{n}) \sum_{b\neq a} \left[\mathcal{G}_{ab}(q\boldsymbol{n}) - \frac{|\mathcal{F}_{ab}(q\boldsymbol{n})|^2}{q^2} \right], \tag{42}$$

where $q = \omega_{ab}/c$ and the integration is over the unit sphere $\boldsymbol{n} \in \mathbb{S}^2$. Note that in the point-dipole limit the quantity $\mathcal{F}_{ab}$ tends to δ_{ab}. In this way, we recover the familiar Weisskopf–Wigner result [52].

The frequency shifts of the atomic levels should be determined using equations (36)–(41), through

$$\Delta_a = \frac{1}{\hbar^2} \sum_b \text{P}\!\int_0^\infty d\omega \frac{T_{ab}(\omega)}{\omega - \omega_{ab}}, \tag{43}$$

with $\text{P}\int$ denoting principal value integration. For $a = b$ the function $\mathcal{T}_{ab}$ contains the state-independent, non-integrable term

$$\delta_{ab} C(\omega)^2 |\boldsymbol{q}|^{-2}(1 - \mathcal{D}(|\boldsymbol{q}|,\omega)) \sim |\boldsymbol{q}|^{-2} \quad \text{as } |\boldsymbol{q}| \to \infty, \tag{44}$$

which provides a divergent contribution to $T_{aa}(\omega)$. However, this contribution is also independent of the state, representing therefore the effect of a uniform energy shift. Physical quantities such as the perturbed transition frequency

$$
\begin{aligned}
\tilde{\omega}_{ab} &= \omega_{ab} + \Delta_a - \Delta_b = \omega_{ab} + \frac{1}{\hbar^2}\text{P}\!\int_0^\infty d\omega \left[\frac{T_{aa}(\omega) - T_{bb}(\omega)}{\omega} \right. \\
&\left. + 2\omega_{ab}\frac{T_{ab}(\omega)}{\omega^2 - \omega_{ab}^2} + \sum_{c\neq a,b} \left(\frac{T_{ac}(\omega)}{\omega - \omega_{ac}} - \frac{T_{bc}(\omega)}{\omega - \omega_{bc}} \right) \right]
\end{aligned}
\tag{45}
$$

are thus independent of the divergent term given in (44). Indeed, notice that, in the time domain the low-energy behavior of the dielectric permittivity is

$$\epsilon(\omega) = 1 + \int_0^\infty dt\, \chi(t) + i\omega \int_0^\infty dt\, t\chi(t) + O(\omega^2), \tag{46}$$

where $\chi(t)$ is the medium susceptibility with finite moments. This implies that $T_{ab}(\omega) \sim \omega$ close to the origin, and therefore the integration of the term $(T_{aa} - T_{bb})/\omega$ in equation (45) is well defined.

3.1. Asymmetric two-level atom

The parity asymmetry of the atomic Hamiltonian eigenstates, reflected by the presence of nonvanishing expectation values of one or more components of $\boldsymbol{r}$, affects the state-dependent quantities $\mathcal{F}_{ab}$ and $\mathcal{G}_{ab}$, which appear in the expression of $T_{ab}(\omega)$ and determine the decay rate Γ_a and the energy shift Δ_a. In a two-level atomic system, the three components of the Hermitian position operator $\boldsymbol{r}$ can be represented by spin operators [52, 53]

$$\boldsymbol{r} = \boldsymbol{\rho}\mathbf{1} + \boldsymbol{\delta}\sigma_z + \boldsymbol{r}_{ab}\sigma_x, \qquad \sigma_x = |a\rangle\langle b| + |b\rangle\langle a|, \qquad \sigma_z = |a\rangle\langle a| - |b\rangle\langle b| \tag{47}$$

acting on the two-dimensional space spanned by $|a\rangle, |b\rangle$, with

$$\boldsymbol{\rho} = \frac{\langle a|\boldsymbol{r}|a\rangle + \langle b|\boldsymbol{r}|b\rangle}{2}, \tag{48}$$

$$\boldsymbol{\delta} = \frac{\langle a|\boldsymbol{r}|a\rangle - \langle b|\boldsymbol{r}|b\rangle}{2}, \tag{49}$$

$$\boldsymbol{r}_{ab} = \langle a|\boldsymbol{r}|b\rangle = \langle b|\boldsymbol{r}|a\rangle. \tag{50}$$

In the two-level case, the off-diagonal matrix element (50) can be made real and non-negative by absorbing a phase factor in the definition of one of the states.

The functions that determine the decay rate from $|a\rangle$ to $|b\rangle$ read

$$\mathcal{F}_{ab}(\boldsymbol{q}) = -\mathrm{i}e^{-\mathrm{i}\boldsymbol{q}\cdot\boldsymbol{\rho}}\boldsymbol{q}\cdot\boldsymbol{r}_{ab}\,\mathrm{sinc}(A(\boldsymbol{q})),$$

$$\mathcal{G}_{ab}(\boldsymbol{q}) = \left|\nabla_{\boldsymbol{q}}\left[\boldsymbol{q}\cdot\boldsymbol{r}_{ab}\int_0^1 \mathrm{d}s\,\mathrm{sinc}(sA(\boldsymbol{q}))e^{-\mathrm{i}s\boldsymbol{q}\cdot\boldsymbol{\rho}}\right]\right|^2, \tag{51}$$

with $\mathrm{sinc}(x) = \sin(x)/x$ and $A(\boldsymbol{q}) = \sqrt{(\boldsymbol{q}\cdot\boldsymbol{r}_{ab})^2 + (\boldsymbol{q}\cdot\boldsymbol{\delta})^2}$.

From these results, one can observe that the physical quantities computed from $\mathcal{G}_{ab}$ and from the square modulus of $\mathcal{F}_{ab}$ are invariant with respect to the inversions $\boldsymbol{\rho} \to -\boldsymbol{\rho}$ and $\boldsymbol{\delta} \to -\boldsymbol{\delta}$, but both depend on diagonal entries $\boldsymbol{\rho}$ and $\boldsymbol{\delta}$ which play the role of the asymmetric contributions.

To identify the lowest-order contributions to the decay rate, let us perform a small-$\boldsymbol{q}$ expansion of the functions appearing in the expression (36) of $\mathcal{T}_{ab}$ for $a \neq b$, namely

$$\frac{|\mathcal{F}_{ab}(\boldsymbol{q})|^2}{|\boldsymbol{q}|^2} \simeq \frac{(\boldsymbol{q}\cdot\boldsymbol{r}_{ab})^2}{|\boldsymbol{q}|^2}\left(1 - \frac{(\boldsymbol{q}\cdot\boldsymbol{r}_{ab})^2 + (\boldsymbol{q}\cdot\boldsymbol{\delta})^2}{6}\right), \tag{52}$$

and

$$\mathcal{G}_{ab}(\boldsymbol{q}) \simeq |\boldsymbol{r}_{ab}|^2\left(1 - \frac{(\boldsymbol{q}\cdot\boldsymbol{r}_{ab})^2}{3} + \frac{(\boldsymbol{q}\cdot\boldsymbol{\delta})^2}{9} + \frac{(\boldsymbol{q}\cdot\boldsymbol{\rho})^2}{12}\right)$$
$$+ \frac{|\boldsymbol{\rho}|^2(\boldsymbol{q}\cdot\boldsymbol{r}_{ab})^2}{4} + (\boldsymbol{q}\cdot\boldsymbol{r}_{ab})\boldsymbol{r}_{ab}\cdot\left(\frac{(\boldsymbol{q}\cdot\boldsymbol{\rho})\boldsymbol{\rho}}{2} - \frac{(\boldsymbol{q}\cdot\boldsymbol{\delta})\boldsymbol{\delta}}{9}\right). \tag{53}$$
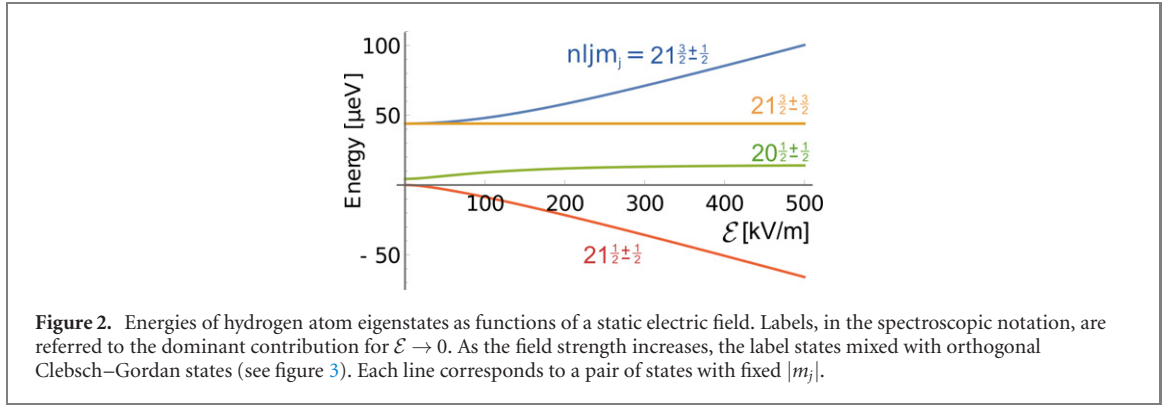
While the first-order contributions are regular, the second-order approximation in $\boldsymbol{q}$ of the functions in equations (52) and (53) yield divergent integrals, that should be regularized by a cutoff $\Lambda_{\boldsymbol{q}}$, roughly corresponding to the inverse spatial size of the involved wavefunctions, that can range from 1 to 100 nm according to the considered system. Clearly, this cutoff is not needed if one uses the expressions in equation (51), that contain all orders in $\boldsymbol{q}$. Based on the approximations (52) and (53), one can estimate that the corrections entailed by an asymmetry of the states $|a\rangle$ and $|b\rangle$ are of order $(\Lambda_{\boldsymbol{q}}|\boldsymbol{r}_{aa}|)^2$ and $(\Lambda_{\boldsymbol{q}}|\boldsymbol{r}_{bb}|)^2$. Notice that the asymmetry corrections compete with terms of order $(\Lambda_{\boldsymbol{q}}|\boldsymbol{r}_{ab}|)^2$, representing the first corrections to the point-dipole result, and are not characterized by a definite sign.

4. Test beds

In this section, we apply the theory to two systems: a hydrogen atom in a static electric field and an asymmetric quantum well (QW). We shall focus on the dependence of spontaneous emission on their spatial asymmetry and on the embedding in an absorptive medium.

4.1. Hydrogen atom in a static electric field

The first example we consider is a hydrogen atom embedded in a homogeneous medium. The asymmetry of this system is related to the presence of a static electric field $\mathcal{E}$, whose polarization defines the quantization

Figure 2. Energies of hydrogen atom eigenstates as functions of a static electric field. Labels, in the spectroscopic notation, are referred to the dominant contribution for $\mathcal{E} \to 0$. As the field strength increases, the label states mixed with orthogonal Clebsch–Gordan states (see figure 3). Each line corresponds to a pair of states with fixed $|m_j|$.

axis. The asymmetry can be classically explained by a shift of the electronic cloud with respect to the nucleus. As a result, the eigenstates of the system perturbed by the field correspond to superpositions of wavefunctions

$$|\psi(\mathcal{E})\rangle = \sum_{nlms} b_{nlms}(\mathcal{E}) |\psi_{nlm}\rangle \otimes |\chi_s\rangle \tag{54}$$

of a bare hydrogen atom, where the orbital wavefunction $|\psi_{nlm}\rangle$ is characterized by the principal (n), angular (l) and magnetic (m) quantum numbers, and $|\chi_s\rangle$ represent the spin up (down) state for $s = +$ ($s = -$). Equivalently, the same state can be decomposed in the Clebsch–Gordan basis
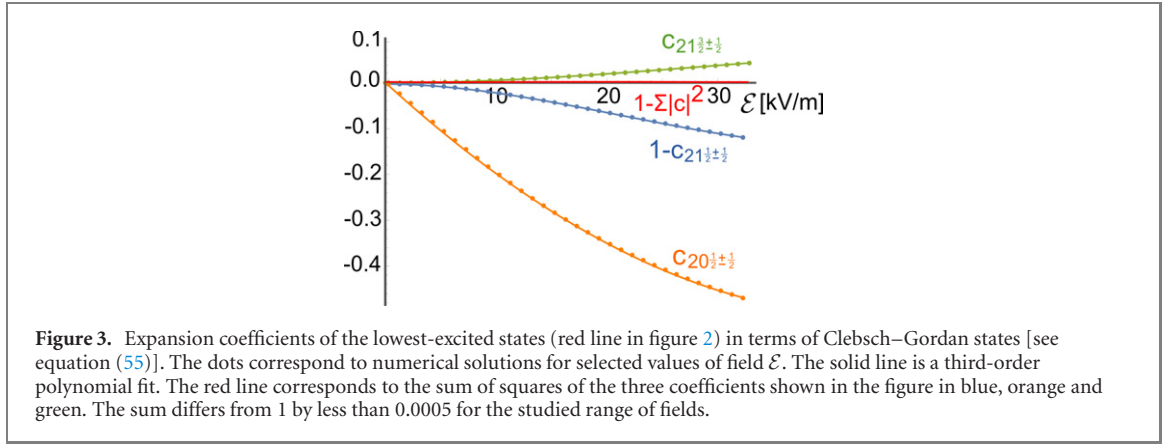
$$|\psi(\mathcal{E})\rangle = \sum_{nljm_j} c_{nljm_j}(\mathcal{E}) |\phi_{nljm_j}\rangle, \tag{55}$$

with j the total angular momentum and m_j its projection on the third axis. Clebsch–Gordan states corresponding to $n = 1, 2$, on which the following analysis will be focused, read

$$|\phi_{10\frac{1}{2}\frac{1}{2}}\rangle = |\psi_{100}\rangle \otimes |\chi_+\rangle,$$

$$|\phi_{10\frac{1}{2}\frac{-1}{2}}\rangle = |\psi_{100}\rangle \otimes |\chi_-\rangle,$$

$$|\phi_{20\frac{1}{2}\frac{1}{2}}\rangle = |\psi_{200}\rangle \otimes |\chi_+\rangle,$$

$$|\phi_{20\frac{1}{2}\frac{-1}{2}}\rangle = |\psi_{200}\rangle \otimes |\chi_-\rangle,$$

$$|\phi_{21\frac{1}{2}\frac{1}{2}}\rangle = \sqrt{\frac{2}{3}}|\psi_{211}\rangle \otimes |\chi_-\rangle - \sqrt{\frac{1}{3}}|\psi_{210}\rangle \otimes |\chi_+\rangle,$$

$$|\phi_{21\frac{1}{2}\frac{-1}{2}}\rangle = -\sqrt{\frac{2}{3}}|\psi_{211}\rangle \otimes |\chi_+\rangle + \sqrt{\frac{1}{3}}|\psi_{210}\rangle \otimes |\chi_-\rangle,$$

$$|\phi_{21\frac{3}{2}\frac{3}{2}}\rangle = |\psi_{211}\rangle \otimes |\chi_+\rangle,$$

$$|\phi_{21\frac{3}{2}\frac{1}{2}}\rangle = \sqrt{\frac{1}{3}}|\psi_{211}\rangle \otimes |\chi_-\rangle + \sqrt{\frac{2}{3}}|\psi_{210}\rangle \otimes |\chi_+\rangle,$$

$$|\phi_{21\frac{3}{2}\frac{-1}{2}}\rangle = \sqrt{\frac{1}{3}}|\psi_{21-1}\rangle \otimes |\chi_+\rangle + \sqrt{\frac{2}{3}}|\psi_{210}\rangle \otimes |\chi_-\rangle,$$

$$|\phi_{21\frac{3}{2}\frac{-3}{2}}\rangle = |\psi_{21-1}\rangle \otimes |\chi_-\rangle. \tag{56}$$

Notice that states $|\phi_{n0jm_j}\rangle$ and $|\phi_{n1jm_j}\rangle$ correspond, in the spectroscopic notation, to ns_{j,m_j} and np_{j,m_j}, respectively. In our analysis we will adapt the discussion from reference [54] to the case of electric fields weak enough to see its gradual influence on the eigenstates. As a consequence, the expansion coefficients depend on the applied field as suggested above in equations (54) and (55). This result is achieved if the corrections induced by the field are small with respect to the fine structure, and comparable with the Lamb shift. In the opposite case of fields strong enough to overcome the fine structure, the eigenstates are fixed and only their energies still depend on the field.

We will now identify the eigenstates in the weak-field regime, and discuss the evaluation of the transition rate between a selected pair of these eigenstates. As anticipated, we restrict the analysis to the $n = 1, 2$ manifolds and neglect the small impact of states with $n > 2$. If one neglects fine-structure splitting and Lamb shift, the eigenenergies of the $n = 1$ and $n = 2$ sectors can be set to

Figure 3. Expansion coefficients of the lowest-excited states (red line in figure 2) in terms of Clebsch–Gordan states [see equation (55)]. The dots correspond to numerical solutions for selected values of field $\mathcal{E}$. The solid line is a third-order polynomial fit. The red line corresponds to the sum of squares of the three coefficients shown in the figure in blue, orange and green. The sum differs from 1 by less than 0.0005 for the studied range of fields.

$\epsilon_1 = -13.6\left(1 - \frac{1}{2^2}\right)$ eV $= -10.2$ eV and $\epsilon_2 = 0$. The Hamiltonian H_0, restricted to the sector spanned by the Clebsch–Gordan basis, ordered as above, is diagonal in the absence of the field, while, in the general case, it reads

$$
H_0 = \begin{pmatrix}
\epsilon_1 & 0 & 0 & 0 & -b_1\mathcal{V} & 0 & 0 & b_2\mathcal{V} & 0 & 0 \\
0 & \epsilon_1 & 0 & 0 & 0 & b_1\mathcal{V} & 0 & 0 & b_2\mathcal{V} & 0 \\
0 & 0 & \Delta_L & 0 & \sqrt{3}\mathcal{V} & 0 & 0 & \sqrt{6}\mathcal{V} & 0 & 0 \\
0 & 0 & 0 & \Delta_L & 0 & -\sqrt{3}\mathcal{V} & 0 & 0 & \sqrt{6}\mathcal{V} & 0 \\
-b_1\mathcal{V} & 0 & \sqrt{3}\mathcal{V} & 0 & 0 & 0 & 0 & 0 & 0 & 0 \\
0 & b_1\mathcal{V} & 0 & -\sqrt{3}\mathcal{V} & 0 & 0 & 0 & 0 & 0 & 0 \\
0 & 0 & 0 & 0 & 0 & 0 & \Delta_{\mathrm{FS}} & 0 & 0 & 0 \\
b_2\mathcal{V} & 0 & \sqrt{6}\mathcal{V} & 0 & 0 & 0 & 0 & \Delta_{\mathrm{FS}} & 0 & 0 \\
0 & b_2\mathcal{V} & 0 & \sqrt{6}\mathcal{V} & 0 & 0 & 0 & 0 & \Delta_{\mathrm{FS}} & 0 \\
0 & 0 & 0 & 0 & 0 & 0 & 0 & 0 & 0 & \Delta_{\mathrm{FS}}
\end{pmatrix}.
$$

Here $\Delta_{\mathrm{FS}} = 44\ \mu$eV and $\Delta_{\mathrm{L}} = 4.4\ \mu$eV represent respectively the fine structure splitting and the Lamb shift for hydrogen, and $\mathcal{V} = \mathcal{E}ea_0$, with e the elementary charge and a_0 the Bohr radius. The constants $b_1 = \frac{128}{243}\sqrt{\frac{2}{3}}$ and $b_2 = \frac{256}{243}\sqrt{\frac{1}{3}}$ and other off-diagonal elements can be evaluated through an explicit calculation of the corrections $-\mathcal{E}e\langle\phi_{10jm_j}|z|\phi_{21j',m_{j'}}\rangle$.
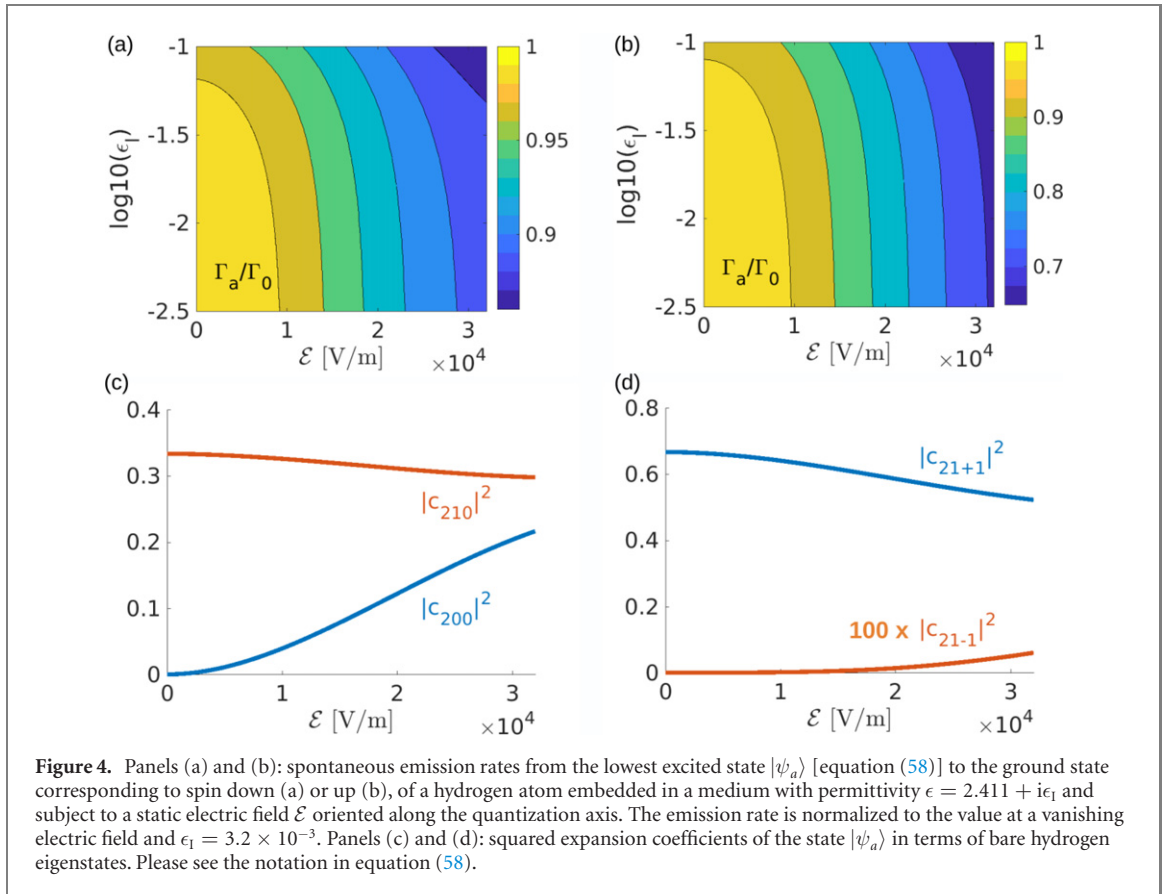
Diagonalizing the above Hamiltonian, we find the eigenstates of the system. Our first observation is that the eigenstates originating at the $n = 1$ manifold are barely distorted by the field, and their energy is shifted by a correction of the order of peV. In the following analysis we neglect these corrections, both in the eigenstate and in its energy. The dependence of eigenenergies of the $n = 2$ manifold on the field is shown in figure 2, and again the influence of states from the $n = 1$ manifold is negligible. For this reason, from now on we consider the Hamiltonian (57) with $b_1 = b_2 = 0$.

From figure 2 it is clear that the pair of lowest-excited states corresponds to the red line and simplifies to the states $2p_{\frac{1}{2},|m_j|=\frac{1}{2}}$ in the absence of the field. The explicit expansion of these eigenstates in terms of Clebsch–Gordan states and in function of the field is cumbersome. Instead, we find the expansion coefficients numerically and fit them with third-order polynomial functions of $\mathcal{E}$ (figure 3). For positive $\mathcal{E}$, the expansion coefficients are

$$
|\psi_{\mathrm{le},\,\mathrm{m}_j}\rangle = c_{21\frac{1}{2}m_j}|\phi_{21\frac{1}{2}m_j}\rangle + c_{20\frac{1}{2}m_j}|\phi_{20\frac{1}{2}m_j}\rangle + c_{21\frac{3}{2}m_j}|\phi_{21\frac{3}{2}m_j}\rangle, \quad (\text{with } \mathrm{m}_j = \pm 1/2)
$$

$$
c_{21\frac{1}{2}m_j}(\mathcal{E}) \approx 1 - 1.28 \times 10^{-7}\frac{\mathrm{m}}{\mathrm{eV}}\mathcal{E} - 2.20 \times 10^{-10}\left(\frac{\mathrm{m}}{\mathrm{eV}}\right)^2\mathcal{E}^2 + 3.49 \times 10^{-15}\left(\frac{\mathrm{m}}{\mathrm{eV}}\right)^3\mathcal{E}^3
$$

$$
c_{20\frac{1}{2}m_j}(\mathcal{E}) \approx -2.20 \times 10^{-5}\frac{\mathrm{m}}{\mathrm{eV}}\mathcal{E} + 2.17 \times 10^{-10}\left(\frac{\mathrm{m}}{\mathrm{eV}}\right)^2\mathcal{E}^2 + 5.10 \times 10^{-16}\left(\frac{\mathrm{m}}{\mathrm{eV}}\right)^3\mathcal{E}^3
$$

$$
c_{21\frac{3}{2}m_j}(\mathcal{E}) \approx 1.19 \times 10^{-9}\frac{\mathrm{m}}{\mathrm{eV}}\mathcal{E} + 6.58 \times 10^{-11}\left(\frac{\mathrm{m}}{\mathrm{eV}}\right)^2\mathcal{E}^2 - 7.63 \times 10^{-16}\left(\frac{\mathrm{m}}{\mathrm{eV}}\right)^3\mathcal{E}^3 \tag{57}
$$

where the subscript 'le' stands for 'lowest-excited'. With the third-order expansion, the state is normalized to 1 with error smaller than 0.05% for $\mathcal{E} < 35$ keV m^{-1}.

There are four possible transitions between a doubly-degenerate excited and a doubly-degenerate ground state. We now select two example transitions among them, namely (i) the transition between the

Figure 4. Panels (a) and (b): spontaneous emission rates from the lowest excited state $|\psi_a\rangle$ [equation (58)] to the ground state corresponding to spin down (a) or up (b), of a hydrogen atom embedded in a medium with permittivity $\epsilon = 2.411 + i\epsilon_I$ and subject to a static electric field $\mathcal{E}$ oriented along the quantization axis. The emission rate is normalized to the value at a vanishing electric field and $\epsilon_I = 3.2 \times 10^{-3}$. Panels (c) and (d): squared expansion coefficients of the state $|\psi_a\rangle$ in terms of bare hydrogen eigenstates. Please see the notation in equation (58).

excited and ground states with $m_j = -\frac{1}{2}$

$$|\psi_a\rangle = |\psi_{\text{le}, m_j = -\frac{1}{2}}\rangle = b_{200\frac{-1}{2}}(\mathcal{E})|\psi_{200}\rangle \otimes |\chi_-\rangle + b_{210\frac{-1}{2}}(\mathcal{E})|\psi_{210}\rangle \otimes |\chi_-\rangle$$
$$+ b_{211\frac{1}{2}}(\mathcal{E})|\psi_{211}\rangle \otimes |\chi_+\rangle + b_{21-1\frac{1}{2}}(\mathcal{E})|\psi_{21-1}\rangle \otimes |\chi_+\rangle, \tag{58}$$

$$|\psi_b\rangle = |\phi_{10\frac{1}{2}\frac{-1}{2}}\rangle = |\psi_{100}\rangle \otimes |\chi_-\rangle, \tag{59}$$

with

$$b_{200\frac{-1}{2}}(\mathcal{E}) = c_{20\frac{1}{2}\frac{-1}{2}}(\mathcal{E}) \tag{60}$$

$$b_{210\frac{-1}{2}}(\mathcal{E}) = \sqrt{\frac{1}{3}}c_{21\frac{1}{2}\frac{-1}{2}}(\mathcal{E}) + \sqrt{\frac{2}{3}}c_{21\frac{3}{2}\frac{-1}{2}}(\mathcal{E}) \tag{61}$$

$$b_{211\frac{1}{2}}(\mathcal{E}) = -\sqrt{\frac{2}{3}}c_{21\frac{1}{2}\frac{-1}{2}}(\mathcal{E}) \tag{62}$$

$$b_{21-1\frac{1}{2}}(\mathcal{E}) = \sqrt{\frac{1}{3}}c_{21\frac{3}{2}\frac{-1}{2}}(\mathcal{E}) \tag{63}$$

and (ii) the transition between the same ψ_a and $\psi_b' = \phi_{10\frac{1}{2}\frac{1}{2}} = \psi_{100}\chi_+$. Please note that, with the approximations described above, the ground state always has a fixed spin, while the excited state has contributions from both spin directions. In each case, the spin-changing transition elements vanish identically.

As the host medium, we consider a glass with the real part of the permittivity $\epsilon_R = 2.411$ [58]. The imaginary part of glass permittivity ϵ_I is physically negligible. For demonstration purposes, we will consider the rather broad range $\epsilon_I \in (10^{-3}, 10^{-1})$.

We now evaluate Γ_a applying the theory developed in section 3 and leading to equation (40). The spontaneous emission rates for both transitions are displayed as functions of the external field $\mathcal{E}$ and the imaginary part of the permittivity ϵ_I in figures 4(a) and (b). As the asymmetry grows the transition rate is reduced in both cases, which is due to the increasing contribution of the 'dark' component ψ_{200} [figures 4(c) and (d)]: a transition between $|\psi_{200}\rangle$ and $|\psi_{100}\rangle$ is electric-dipole forbidden. We observe that

the emission weakly depends on the absorption coefficient and slightly drops for larger values of the latter.

We remark that, albeit these results have been obtained under the assumption of a homogeneous medium, which does not fully describe the physics of a system as small as a hydrogen atom, our analysis captures crucial information on the trends of the relevant physical quantities.

4.2. Asymmetric quantum well

We evaluate here the decay rate for a semiconductor QW. We consider the case of a symmetric and an asymmetric QW embedded in the same surrounding material.

The considered QW consists of aluminium indium arsenide with different molar fractions ($Al_xIn_{1-x}As$ and $Al_zIn_{1-z}As$) and gallium indium arsenide ($Ga_yIn_{1-y}As$), with $x = 0.46, y = 0.48, z = 0.47$, respectively. The well has a finite length a. The effective mass in the three regions is $m = 0.043m_e$, $m = 0.045m_e$ and $m = 0.078m_e$, respectively, where m_e is the electron mass. By varying the molar fractions it is possible to modify the height of potential barriers $V_{L/R}$ on the left/right side of the QW, and consequently confine the electron along the x-direction with a potential [55]

$$V(x) = \begin{cases} V_L & \text{for } x < -a/2 \\ 0 & \text{for } -a/2 \leqslant x \leqslant a/2 \\ V_R & \text{for } x > a/2. \end{cases} \tag{64}$$

Motion along the transverse (y, z) directions is loosely bound; for simplicity, we will assume a weak harmonic confinement along those directions. The asymmetry of the system is related to the nonvanishing value of $V_R - V_L$ along the x-axis. In GaInAs, $V_R = 520$ meV and V_L can be tuned with a sensitivity of 3 meV [56, 57]. The energy spectrum is determined by the following equation

$$a\sqrt{\frac{2mE}{\hbar^2}} = n\pi - \arcsin\sqrt{\frac{E}{V_L}} - \arcsin\sqrt{\frac{E}{V_R}}, \tag{65}$$

where $n = 1, 2$ correspond to the ground and the excited state, respectively. By tuning V_L, one can set the energy gap between the two lowest levels. We set the QW width a to ensure the absence of a third bound level, as shown in figure 5, and approximate our dynamics with the one of a two-level system. Typically, a can be controlled with a precision of half a constant lattice 0.3 nm [56]. The wavefunctions ψ_n, corresponding to the energy eigenvalues E_n, with $n \geqslant 1$, are given by

$$\Psi_n(x) = c_n \begin{cases} \sin(\delta_n)e^{\alpha_{nL}\left(x+\frac{a}{2}\right)} & \text{for } x < -\frac{a}{2} \\ \sin(\beta_n(x + \frac{a}{2}) + \delta_n) & \text{for } -\frac{a}{2} \leqslant x \leqslant \frac{a}{2}, \\ \sin(a\beta_n + \delta_n)e^{-\alpha_{nR}\left(x-\frac{a}{2}\right)} & \text{for } x > \frac{a}{2} \end{cases} \tag{66}$$

where $\alpha_{nR(nL)} = \sqrt{2m\left(V_{R(L)} - E_n\right)}/\hbar$, $\beta_n = \sqrt{2mE_n}/\hbar$, $\delta_n = \text{arccot}\left(\alpha_{nL}/\beta_n\right)$ and c_n is a normalization constant.

The structure of the QW entails a trade-off between its width and the resonance wavelength λ (see figure 6) corresponding to the energy gap. The larger the width a, the larger the resonant wavelength, but the complex part of the permittivity becomes drastically smaller. This yields a medium that is practically transparent. For GaInAs, the relative permittivity is given by $\epsilon_R = 11.638$ and $\epsilon_I = 0.024\,082$ at the resonance energy gap of 161.917 meV determined by $V_L = 430$ meV.

We consider the spontaneous transition between two states a and b, characterized by the wavefunctions
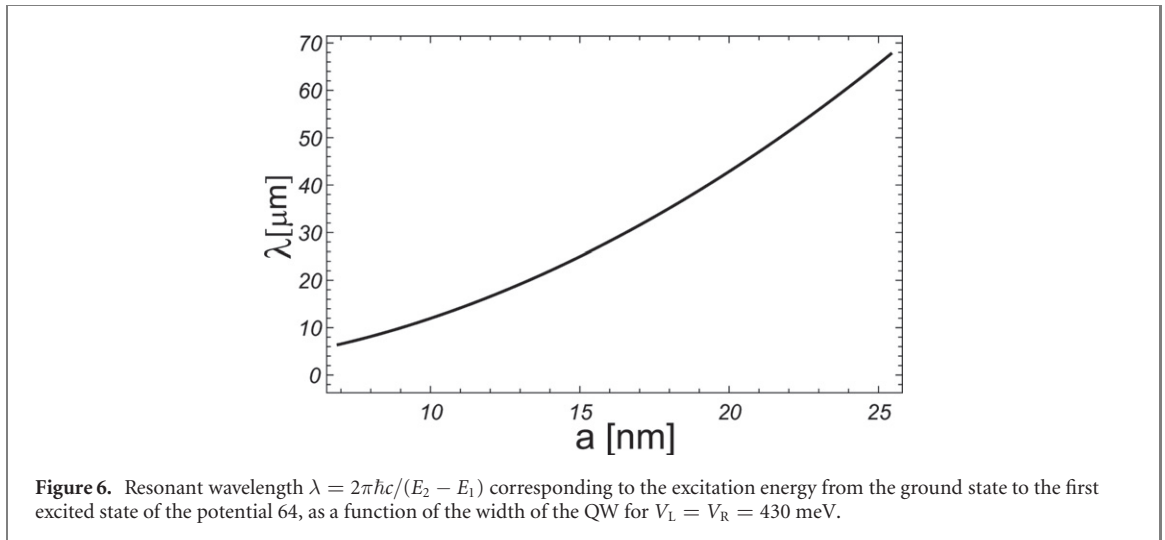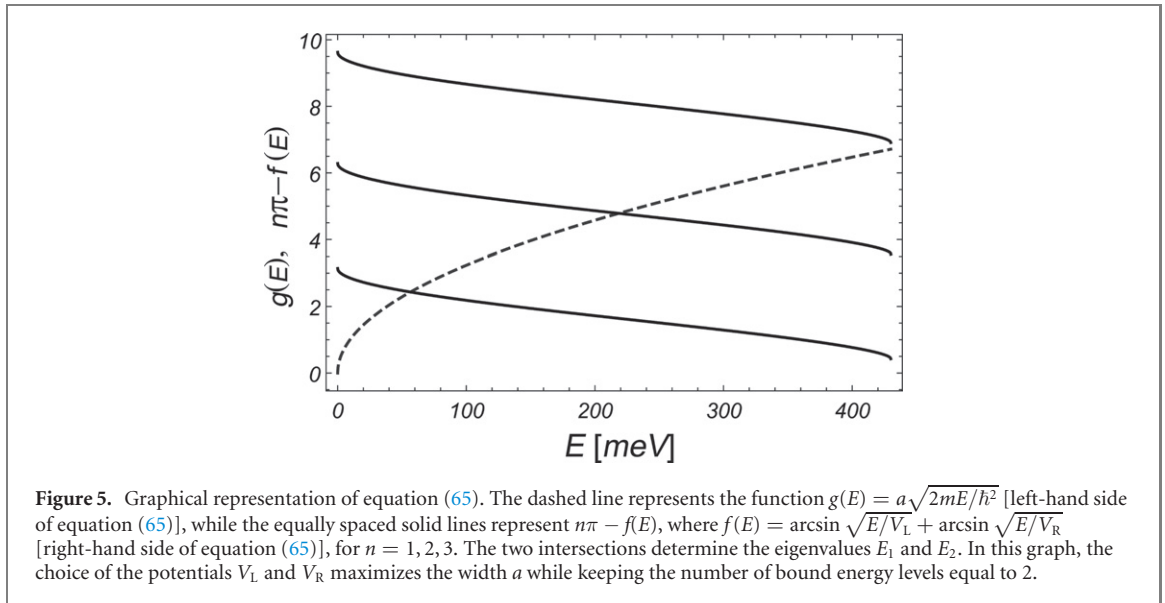
$$\psi_a(\mathbf{r}) = \Psi_2(-x)\frac{e^{-\frac{y^2+z^2}{4\sigma^2}}}{\sqrt{2\pi\sigma^2}}, \qquad \psi_b(\mathbf{r}) = \Psi_1(-x)\frac{e^{-\frac{y^2+z^2}{4\sigma^2}}}{\sqrt{2\pi\sigma^2}}, \tag{67}$$

where the Gaussian part in the (y, z) variables is related to the weak harmonic transverse confinement. Since the transverse wavefunction is the same for a and b, the matrix elements of the dipole moment only have components along x:

$$e\begin{pmatrix} x_{aa} & x_{ab} \\ x_{ba} & x_{bb} \end{pmatrix} = \begin{pmatrix} 0.007 & 0.213 \\ 0.213 & 0.0153 \end{pmatrix}ea_0, \tag{68}$$

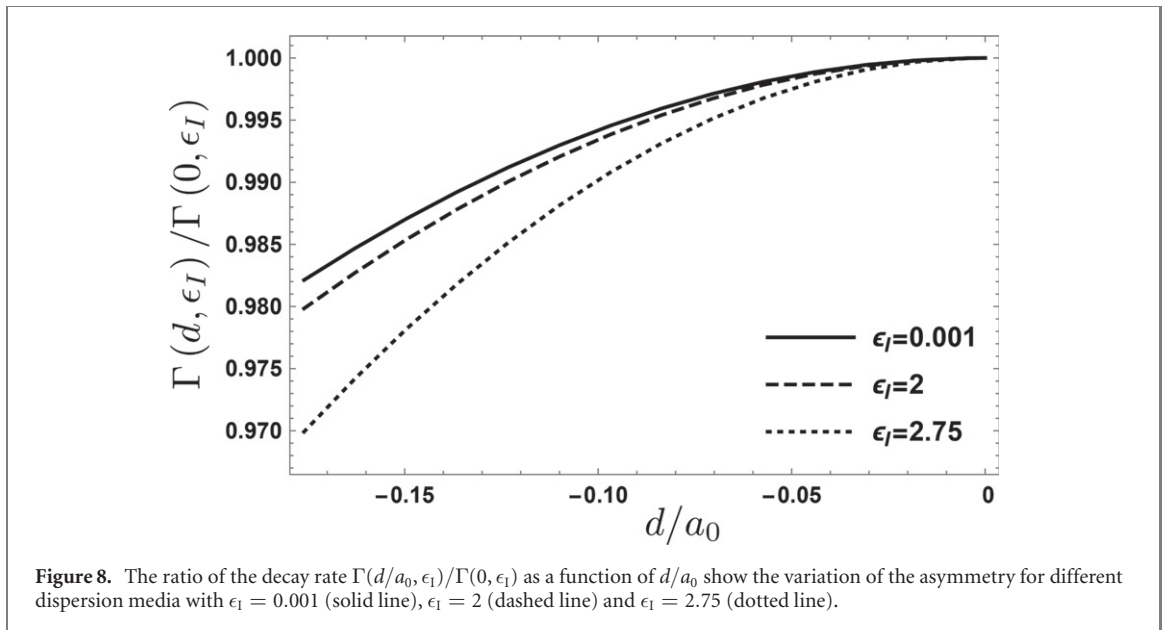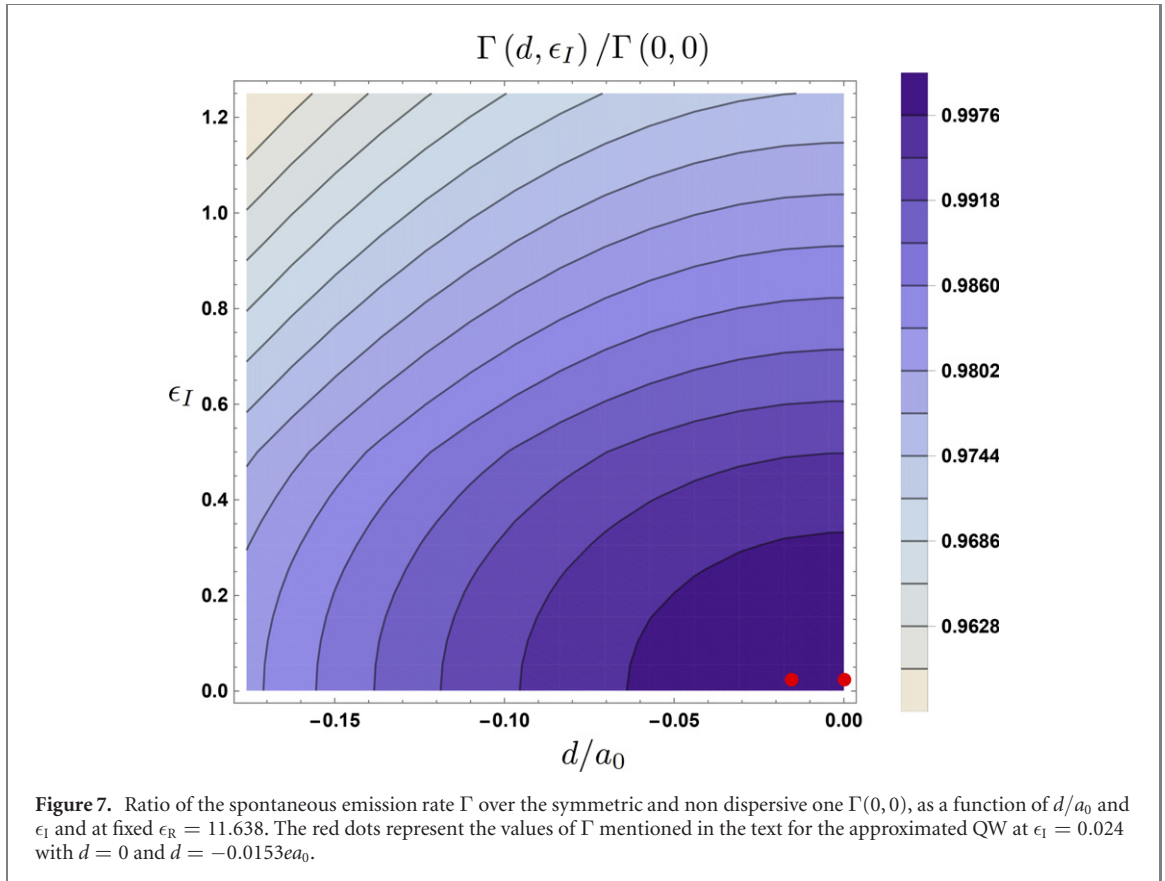with $e = 1.60 \times 10^{-19}$ C the electron charge and $a_0 = 5.29 \times 10^{-11}$ m the Bohr radius.

Unlike the case of the hydrogen atom, discussed in section 4.1, here both functions are characterized by a finite dipole moment. In order to highlight the specific effects of the average dipole moment of the two

Figure 5. Graphical representation of equation (65). The dashed line represents the function $g(E) = a\sqrt{2mE/\hbar^2}$ [left-hand side of equation (65)], while the equally spaced solid lines represent $n\pi - f(E)$, where $f(E) = \arcsin\sqrt{E/V_L} + \arcsin\sqrt{E/V_R}$ [right-hand side of equation (65)], for $n = 1, 2, 3$. The two intersections determine the eigenvalues E_1 and E_2. In this graph, the choice of the potentials V_L and V_R maximizes the width a while keeping the number of bound energy levels equal to 2.

Figure 6. Resonant wavelength $\lambda = 2\pi\hbar c/(E_2 - E_1)$ corresponding to the excitation energy from the ground state to the first excited state of the potential 64, as a function of the width of the QW for $V_L = V_R = 430$ meV.

states [see equation (48)], we will consider an approximation in which the wavefunctions (66) are replaced by harmonic oscillator eigenfunctions, both characterized by the same permanent dipole moment $\mu = ex_{aa} = ex_{bb}$. The frequency ω_{ho} of the harmonic oscillator is fixed in such a way that $\hbar\omega_{ho}$ matches the excitation energy from the ground state to the first excited state of the QW. The permanent dipole μ for the harmonic oscillator is obtained by shifting its wavefunctions along the x-axis such that $\mu = 0.0153ea_0$. Hence,

$$\Psi_1(-x) \simeq \frac{e^{-\frac{(x+x_{aa})^2}{4\sigma_x^2}}}{\sqrt[4]{2\pi\sigma_x^2}}, \qquad \Psi_2(-x) \simeq \frac{x+x_{aa}}{\sigma_x} \frac{e^{-\frac{(x+d)^2}{4\sigma_x^2}}}{\sqrt[4]{2\pi\sigma_x^2}} \tag{69}$$

with $\sigma_x^2 = \hbar/(2m\omega_{ho})$. We obtain the decay rates $\Gamma(d = -0.0153ea_0) = 3.297\,08 \times 10^{15}$ s^{-1} and $\Gamma(d = 0) = 3.297\,73 \times 10^{15}$ s^{-1}, yielding a 0.02% increase of the asymmetric case compared to the symmetric one, of the same order of the ratio $d/(ea_0)$ [see equations (52) and (53) and comments thereto]. In figure 7, we show the results for the spontaneous emission rate with varying d and ϵ_I, at fixed $\epsilon_R = 11.638$ of gallium indium arsenide [59]. In vacuum ($\epsilon \to 1$), the relative contribution of the asymmetry to the total decay rate becomes less relevant. Furthermore, to highlight the specific effect of a finite dipole moment, we show in figure 8 the ratio between the value of the decay rate as a function of d and its value for $d = 0$, corresponding to a fixed ϵ_I.

Figure 7. Ratio of the spontaneous emission rate Γ over the symmetric and non dispersive one $\Gamma(0,0)$, as a function of d/a_0 and ϵ_I and at fixed $\epsilon_R = 11.638$. The red dots represent the values of Γ mentioned in the text for the approximated QW at $\epsilon_I = 0.024$ with $d = 0$ and $d = -0.0153ea_0$.

Figure 8. The ratio of the decay rate $\Gamma(d/a_0, \epsilon_I)/\Gamma(0, \epsilon_I)$ as a function of d/a_0 show the variation of the asymmetry for different dispersion media with $\epsilon_I = 0.001$ (solid line), $\epsilon_I = 2$ (dashed line) and $\epsilon_I = 2.75$ (dotted line).

5. Conclusions

We have expressed a light–matter interaction Hamiltonian in terms of the Green tensor propagator, in a novel approach that avoids the usual divergence related to the approximation of a point-like atomic quantum system. The divergence was lifted via the inclusion of the wavefunctions, providing in this way a natural cutoff for the system investigated. This enabled us to study the dynamics of a charged system coupled to a medium-assisted electric field, beyond the point-dipole approximation, highlighting the role played by the finite size of the system, the dispersion and absorption by the medium and the spatial asymmetries. The analysis focused on the determination of the decay rates and energy shifts of the bound states of the 'atomic' system, which have been obtained under general assumptions. The most important

among these assumptions is the hypothesis of homogeneous and isotropic media. We also discussed how to extend the theory to more general situations.

The obtained results were applied to two test-beds: a microscopic one, represented by a hydrogen atom subject to a uniform electric field, and a mesoscopic one, consisting of a quasi-electron in a semiconductor QW. In both cases, we have obtained the decay rates as functions of the asymmetry of the system and the absorption of the medium, showing that asymmetry can yield small but detectable deviations with respect to the symmetric case.

Future research will be devoted to a thorough treatment of medium inhomogeneity and anisotropy and, in particular, to the inclusion of effects due to the medium granularity, which implies a further length scale and momentum cutoff, competing with those related to the atomic system size.

Acknowledgments

ORCID iDs

Giovanni Scala ⓘ https://orcid.org/0000-0003-2685-0946
Francesco V Pepe ⓘ https://orcid.org/0000-0002-7407-063X
Paolo Facchi ⓘ https://orcid.org/0000-0001-9152-6515
Saverio Pascazio ⓘ https://orcid.org/0000-0002-7214-5685
Karolina Słowik ⓘ https://orcid.org/0000-0003-1314-7004

References

[1] Lamb W E and Retherford R C 1947 Fine structure of the hydrogen atom by a microwave method *Phys. Rev.* **72** 241–3
[2] Einstein A 1917 Zur quantentheorie der strahlung *Phys. Z.* **18** 121–8
[3] Kossakowski A 2002 On Markovian limit in quantum open systems *Open Syst. Inf. Dyn.* **9** 1–18
[4] Crespi A, Pepe F V, Facchi P, Sciarrino F, Mataloni P, Nakazato H, Pascazio S and Osellame R 2019 Experimental investigation of quantum decay at short, intermediate, and long times via integrated photonics *Phys. Rev. Lett.* **122** 130401
[5] Pepe F V, Facchi P, Kordi Z and Pascazio S 2020 Nonexponential decay of Feshbach molecules *Phys. Rev.* A **101** 013632
[6] Philbin T G, Xiong C and Leonhardt U 2010 Casimir stress in an inhomogeneous medium *Ann. Phys., NY* **325** 579–95
[7] Dicke R H 1954 Coherence in spontaneous radiation processes *Phys. Rev.* **93** 99–110
[8] Milonni P W 1994 *The Quantum Vacuum: An Introduction to Quantum Electrodynamics* (New York: Academic)
[9] Hillery M and Mlodinow L D 1984 Quantization of electrodynamics in nonlinear dielectric media *Phys. Rev.* A **30** 1860–5
[10] Hillery M and Mlodinow L 1997 Quantized fields in a nonlinear dielectric medium: a microscopic approach *Phys. Rev.* A **55** 678–89
[11] Purcell E M, Torrey H C and Pound R V 1946 Resonance absorption by nuclear magnetic moments in a solid *Phys. Rev.* **69** 37
[12] Akselrod G M, Argyropoulos C, Hoang T B, Ciracì C, Fang C, Huang J, Smith D R and Mikkelsen M H 2014 Probing the mechanisms of large Purcell enhancement in plasmonic nanoantennas *Nat. Photon.* **8** 835–40
[13] Zhang J L *et al* 2018 Strongly cavity-enhanced spontaneous emission from silicon-vacancy centers in diamond *Nano Lett.* **18** 1360–5
[14] Tokman M, Long Z, AlMutairi S, Wang Y, Belkin M and Belyanin A 2018 Enhancement of the spontaneous emission in subwavelength quasi-two-dimensional waveguides and resonators *Phys. Rev.* A **97** 043801
[15] Dzsotjan D, Sørensen A S and Fleischhauer M 2010 Quantum emitters coupled to surface plasmons of a nanowire: a Green's function approach *Phys. Rev.* B **82** 075427
[16] Sinha K, Venkatesh B P and Meystre P 2018 Collective effects in Casimir–Polder forces *Phys. Rev. Lett.* **121** 183605
[17] Chikkaraddy R *et al* 2016 Single-molecule strong coupling at room temperature in plasmonic nanocavities *Nature* **535** 127–30
[18] Benz F *et al* 2016 Single-molecule optomechanics in picocavities *Science* **354** 726–9
[19] Stobbe S, Kristensen P T, Mortensen J E, Hvam J M, Mørk J and Lodahl P 2012 Spontaneous emission from large quantum dots in nanostructures: exciton–photon interaction beyond the dipole approximation *Phys. Rev.* B **86** 085304
[20] Rivera N, Kaminer I, Zhen B, Joannopoulos J D and Soljačić M 2016 Shrinking light to allow forbidden transitions on the atomic scale *Science* **353** 263–9
[21] Neuman T, Esteban R, Casanova D, García-Vidal F J and Aizpurua J 2018 Coupling of molecular emitters and plasmonic cavities beyond the point-dipole approximation *Nano Lett.* **18** 2358–64

[22] Kosik M, Burlayenko O, Rockstuhl C, Fernandez-Corbaton I and Słowik K 2020 Interaction of atomic systems with quantum vacuum beyond electric dipole approximation *Sci. Rep.* **10** 5879

[23] Kibis O V, Slepyan G Y, Maksimenko S A and Hoffmann A 2009 Matter coupling to strong electromagnetic fields in two-level quantum systems with broken inversion symmetry *Phys. Rev. Lett.* **102** 023601

[24] Savenko I G, Kibis O V and Shelykh I A 2012 Asymmetric quantum dot in a microcavity as a nonlinear optical element *Phys. Rev.* A **85** 053818

[25] Chestnov I Y, Shahnazaryan V A, Alodjants A P and Shelykh I A 2017 Terahertz lasing in ensemble of asymmetric quantum dots *ACS Photonics* **4** 2726–37

[26] Koppenhöfer M and Marthaler M 2016 Creation of a squeezed photon distribution using artificial atoms with broken inversion symmetry *Phys. Rev.* A **93** 023831

[27] Marthaler M, Koppenhöfer M, Słowik K and Rockstuhl C 2016 Lasing at arbitrary frequencies with atoms with broken inversion symmetry and an engineered electromagnetic environment (arXiv:1601.01511)

[28] Avetissian H K and Mkrtchian G F 2013 Two-level system with broken inversion symmetry coupled to a quantum harmonic oscillator *Phys. Rev.* A **88** 043811

[29] Paspalakis E, Boviatsis J and Baskoutas S 2013 Effects of probe field intensity in nonlinear optical processes in asymmetric semiconductor quantum dots *J. Appl. Phys.* **114** 153107

[30] Bimberg D *et al* 2009 Quantum dots for single- and entangled-photon emitters *IEEE Photonics J.* **1** 58–68

[31] Brode W R and Brooks R E 1941 Optically active dyes. V. Molecular asymmetry in dyes and their dyeing properties *J. Am. Chem. Soc.* **63** 923–5

[32] Stables L A, Kennan R P and Gore J C 1998 Asymmetric spin-echo imaging of magnetically inhomogeneous systems: theory, experiment, and numerical studies *Magn. Reson. Med.* **40** 432–42

[33] Martinez-Linares J and Vargas-Medina J 2003 Duality in asymmetric quantum optical Ramsey interferometers (arXiv:quant-ph/0309006)

[34] Doherty M W, Manson N B, Delaney P, Jelezko F, Wrachtrup J and Hollenberg L C L 2013 The nitrogen-vacancy colour centre in diamond *Phys. Rep.* **528** 1–45

[35] Ilani S, Martin J, Teitelbaum E, Smet J H, Mahalu D, Umansky V and Yacoby A 2004 The microscopic nature of localization in the quantum Hall effect *Nature* **427** 328–32

[36] Degen C L, Reinhard F and Cappellaro P 2017 Quantum sensing *Rev. Mod. Phys.* **89** 035002

[37] Buhmann S Y 2012 *Dispersion Forces I* (Berlin: Springer)

[38] Hnizdo V 2004 Regularization of the second-order partial derivatives of the Coulomb potential of a point charge (arXiv:physics/0409072)

[39] Paknys R 2016 *Applied Frequency-Domain Electromagnetics* (New York: Wiley)

[40] Scheel S, Knöll L and Welsch D-G 1999 Spontaneous decay of an excited atom in an absorbing dielectric *Phys. Rev.* A **60** 4094–104

[41] Barnett S M, Huttner B, Loudon R and Matloob R 1996 Decay of excited atoms in absorbing dielectrics *J. Phys. B: At. Mol. Opt. Phys.* **29** 3763

[42] Ho S-T and Kumar P 1993 Quantum optics in a dielectric: macroscopic electromagnetic-field and medium operators for a linear dispersive lossy medium—a microscopic derivation of the operators and their commutation relations *J. Opt. Soc. Am.* B **10** 1620

[43] Qin Q-H 2007 *Green's Function and Boundary Elements of Multifield Materials* (Amsterdam: Elsevier)

[44] Van Bladel J G 2007 *Electromagnetic Fields* (New York: Wiley)

[45] Griffiths D J 2017 *Introduction to Electrodynamics* (Cambridge: Cambridge University Press)

[46] Vogel W and Welsch D-G 2006 *Quantum Optics* (New York: Wiley)

[47] Cohen-Tannoudji C, Dupont-Roc J and Grynberg G 1997 *Photons and Atoms: Introduction to Quantum Electrodynamics* (New York: Wiley)

[48] Huttner B and Barnett S M 1992 Quantization of the electromagnetic field in dielectrics *Phys. Rev.* A **46** 4306–22

[49] Ho T D, Ludwig K and Welsch D-G 2000 Spontaneous decay in the presence of dispersing and absorbing bodies: general theory and application to a spherical cavity *Phys. Rev.* A **62** 053804

[50] Juzeliūnas G 1997 Spontaneous emission in absorbing dielectrics: a microscopic approach *Phys. Rev.* A **55** R4015

[51] Scheel S, Knöll L, Welsch D-G and Barnett S M 1999 Quantum local-field corrections and spontaneous decay *Phys. Rev.* A **60** 1590

[52] Cohen-Tannoudji C, Dupont-Roc J and Grynberg G 1998 *Atom-Photon Interactions: Basic Processes and Applications* (New York: Wiley)

[53] Feynman R P, Leighton R B and Sands M 1964 *The Feynman Lectures on Physics* (Reading, MA: Addison-Wesley)

[54] Cohen-Tannoudji C, Diu B and Laloe F 1977 *Quantum Mechanics* (New York: Wiley)

[55] Landau L D and Lifshitz E M 1981 *Quantum Mechanics: Non-Relativistic Theory* 3rd edn (Portsmouth, NH: Heinemann)

[56] Scamarcio G, Capasso F, Sirtori C, Faist J, Hutchinson A L, Sivco D L and Cho A Y 1997 High-power infrared (8-micrometer wavelength) superlattice lasers *Science* **276** 773–6

[57] Vitiello M S, Gresch T, Lops A, Spagnolo V, Scamarcio G, Hoyler N, Giovannini M and Faist J 2007 Influence of InAs, AlAs δ layers on the optical, electronic, and thermal characteristics of strain-compensated GaInAs/AlInAs quantum-cascade lasers *Appl. Phys. Lett.* **91** 161111

[58] Schott Optical Glass Data Sheets (https://refractiveindex.info/download/data/2017/schott_2017-01-20.pdf) Accessed: 18 November 2020

[59] Adachi S 1989 Optical dispersion relations for GaP, GaAs, GaSb, InP, InAs, InSb, $Al_xGa_{1-x}As$, and $In_{1-x}Ga_xAs_yP_{1-y}$ *J. Appl. Phys.* **66** 6030–40